To appear in Publications of the Astronomical Society of the Pacific 2016

Preprint typeset using LaTeX style AASTeX6 v. 1.0

arXiv:1606.05217v1 [astro-ph.IM] 16 Jun 2016

LOLAS-2: REDESIGN OF AN OPTICAL TURBULENCE PROFILER WITH HIGH ALTITUDE-RESOLUTION

R. Avila,[1] C. A. Zũniga,[1] J. J. Tapia-Rodríguez,[2,1] L. J. Sánchez,[3] I. Cruz-González,[3] J. L. Avilés,[4] O. Valdés-Hernández,[1] and E. Carrasco[4]

[1]Centro de Física Aplicada y Tecnología Avanzada, UNAM, Campus Juriquilla, Apdo. Postal 1-1010, 76000 Querétaro, México.

[2]Instituto Tecnológico de Morelia, Apdo. Postal 262, 58120 Morelia, Michoacán, México.

[3]Instituto de Astronomía, UNAM, Apdo. Postal 70-264, 04510 México D.F., México.

[4]Instituto Nacional de Astrofísica, Óptica y Electrónica, Apdo. Postal 51 y 216, 72840 San Andrés Cholula, Puebla, México.

ABSTRACT

We present the development, tests and first results of the second generation Low Layer Scidar (LOLAS-2). This instrument constitutes a strongly improved version of the prototype Low Layer Scidar, which is aimed at the measurement of optical turbulence profiles close to the ground, with high altitude-resolution. The method is based on the Generalised Scidar principle which consists in taking double-star scintillation images on a defocused pupil plane and calculating in real time the autocovariance of the scintillation. The main components are an open-truss 40-cm Ritchey-Chrétien telescope, a german-type equatorial mount, an Electron Multiplying CCD camera and a dedicated acquisition and real-time data processing software. The new optical design

of LOLAS-2 is significantly simplified compared with the prototype. The experiments carried out to test the permanence of the image within the useful zone of the detector and the stability of the telescope focus show that LOLAS-2 can function without the use of the autoguiding and autofocus algorithms that were developed for the prototype version. Optical turbulence profiles obtained with the new Low Layer Scidar have the best altitude-resolution ever achieved with Scidar-like techniques (6.3 m). The simplification of the optical layout and the improved mechanical properties of the telescope and mount make of LOLAS-2 a more robust instrument.

Keywords: Physical processes: turbulence; Instrumentation: atmospheric effects; Data Analysis and Techniques: site testing; telescopes

1. INTRODUCTION

Turbulent flows in the atmosphere combined with stratified temperatures provoke turbulent fluctuations of the refractive index of air, commonly known as optical turbulence. The intensity of such fluctuations is determined by the second order structure constant C_N^2. The measurement of $C_N^2(h)$, h being the altitude, is of major importance for the development of novel adaptive optical (AO) systems that overcome the angular-resolution degradation introduced by optical turbulence. The statistical study of optical turbulence profiles is also crucial for the characterization of sites where next generation of optical telescopes are to be installed (e.g., Schöck et al. (2009)).

One important limitation of AO systems that are designed to account for phase fluctuations generated all along the atmosphere is the tiny field of view over which the wavefront is corrected. One way to improve image quality over a wide field of view is to correct only the wavefront perturbations that come from turbulent layers close to the ground. This method is known as ground-layer adaptive optics (GLAO) (Rigaut 2002; Tokovinin 2004). Indeed, the compensation of lower-altitude turbulent-layers

provides wider corrected fields of view (Chun 1998) and turbulence close to the ground is generally the most intense (e.g., Avila et al. (2004)). To develop a GLAO system for a given site, it is required to have as much knowledge as possible about the vertical distribution of optical turbulence in the ground layer (e.g, Le Louarn & Hubin (2006)). This requires measurements of $C_N^2(h)$ with very high altitude-resolution close to the ground.

Scintillation Detection and Ranging (SCIDAR) has extensively been used for C_N^2 profiling since its invention by Rocca et al. (1974). The generalised version of the SCIDAR made it possible to detect turbulence near the ground (Fuchs et al. 1998; Avila et al. 1997). A more recent implementation of the Generalized SCIDAR on a 40-cm telescope that used a widely-separated double star as a light source and an Electron Multiplying Charge Coupled Device (EMCCD) as the detector, gave place to the Low Layer SCIDAR (LOLAS) (Avila et al. 2008). The LOLAS prototype was used to characterize the ground-layer turbulence at Mauna Kea, together with a Slope Detection and Ranging instrument (Chun et al. 2009). Although this several-years campaign gave definitive results, the experience showed that a number of aspects on the prototype LOLAS could be improved in order to optimize data acquisition. In this paper we describe the development and tests of the second generation Low Layer Scidar (LOLAS-2).

A few instruments based on optical methods have been developed to measure $C_N^2(h)$ profiles with the required vertical resolution close to the ground. For example, the surface-layer Slope Detection and Ranging (SL-SLODAR) (Osborn et al. 2010) makes use of two Shack-Hartmann wavefront sensors, each looking at one component of a widely-separated double star. The slope of the wavefronts coming from each star is measured on 5-cm square subapertures whereas LOLAS-2 measures scintillation on square elements of 1-cm side approximately, which makes the SL-SLODAR five times more sensitive than the LOLAS-2 for equal integration times or five times faster for equal number of photons per element. On the other hand, if the instruments were using the same double star separation,

LOLAS-2 provides 5 times better altitude resolution. A similar concept that also uses a double star but measures the scintillation from each component on two cameras was implemented in the Stereo-Scidar by Shepherd et al. (2014). The Lunar Scintillometer, which consists of an array of photodiodes that measure scintillation from the moon, has been used to obtain high altitude-resolution turbulence profiles near the ground (Tokovinin et al. 2010). Egner & Masciadri (2007) use a Generalized SCIDAR to distinguish layers at very similar altitudes but moving at different velocities.

The present paper is organized as follows: § 2 gives an overview of the LOLAS method. In § 3.1 we briefly describe the prototype version of the instrument and in § 3.2 the second generation of the instrument is presented. Tests on the instrument performances and some measurements are shown in § 4 and § 5. Conclusions are given in § 6.

2. METHOD

The Low Layer Scidar is based on the principle of the Generalized Scintillation Detection and Ranging (G-SCIDAR) technique (Rocca et al. 1974; Fuchs et al. 1998; Avila et al. 1997). In this section, we present a brief overview of the LOLAS method, since a complete description can be found in Avila et al. (2008). The G-SCIDAR principle can be summarized as follows: double-star scintillation patterns are recorded on short exposure-time images on a virtual plane located a distance $h_{\rm gs}$ from the telescope pupil. In G-SCIDAR experiments this virtual plane is located below the telescope pupil, thus $h_{\rm gs} < 0$. A schematic view of the optical setup is shown in Fig. 1. Each image consists of a randomly distributed intensity pattern. The autocovariance of this stochastic illumination is obtained by computing the spatial normalized autocorrelation of each image and averaging those autocorrelations over thousands of statistically independent image samples. Each layer of optical turbulence contributes to the resulting scintillation autocovariance with three covariance peaks: one centred at the autocovariance origin and two others, identical to each other,

separated from the origin by $\mathbf{d}_\mathrm{l} = -\boldsymbol{\rho}|h - h_\mathrm{gs}|$ and $\mathbf{d}_\mathrm{r} = \boldsymbol{\rho}|h - h_\mathrm{gs}|$, respectively, where $\boldsymbol{\rho}$ denotes the angular separation of the double star and h the layer altitude above the ground. Knowing $\boldsymbol{\rho}$ and the conjugation altitude h_gs, the experimental determination of $\mathbf{d}_\mathrm{l}$ (or $\mathbf{d}_\mathrm{r}$) leads to an estimate of the layer altitude h. The measured autocovariance peaks $C_\mathrm{gs}(\mathbf{r})$ are proportional to the optical turbulence strength at altitude h, $C_\mathrm{N}^2(h)$, and to the scintillation autocovariance function $K(\mathbf{r}, |h - h_\mathrm{gs}|)$. In the realistic case of multiple layers, the response of each layer adds up to the measured autocovariance, resulting in Eq. 1 of Avila et al. (2008). This equation consists of an integral with respect the altitude h that is similar to a convolution, except that the kernel $K(\mathbf{r}, |h - h_\mathrm{gs}|)$ depends on the integration variable. One needs to invert this integral equation to retrieve $C_\mathrm{N}^2(h)$. Due to its similarity with a convolution integral, we developed an algorithm based on the CLEAN method, but in which the kernel is recalculated for each different value of h. Our modified CLEAN algorithm is based on that reported by Prieur et al. (2001). As explained by Avila et al. (2008), the achievable altitude resolution using the modified CLEAN method, when the target is at the zenith is $\Delta h = 0.52\sqrt{\lambda(|h - h_\mathrm{gs}|)}/\rho$, where λ is the wavelength and $\rho = |\boldsymbol{\rho}|$. When the star is located at an elevation angle θ, Δh is decreased by a factor $\cos\theta$. We take $\lambda = 0.5\mu$m, which corresponds to the maximum sensitivity of our detector. For a telescope having an aperture D, the maximum altitude for which the C_N^2 value can be measured is given by $h_\mathrm{max} = D/\rho$ (Avila et al. 2008).

The Low Layer Scidar concept consists of putting into practice a G-SCIDAR on a dedicated portable telescope, using widely separated double stars as light sources. As can be seen from the above expressions for Δh and h_max, the wider the separation, the better the altitude resolution but the shorter the maximum altitude. LOLAS was designed to use a 40-cm telescope, an EMCCD to improve sensitivity and a real-time computation of the scintillation autocovariance. Sections 3.1 and 3.2 describe the prototype LOLAS version and the second generation instrument, respectively.

3. LOLAS INSTRUMENT DEVELOPMENT

3.1. *Prototype version*

The instrumental setup of LOLAS has been widely explained elsewhere (Avila et al. 2008; Chun et al. 2009; Avilés et al. 2012). We present a summary of the most important instrumental characteristics. Figure 2 shows a schematic view of the prototype LOLAS. The scintillation images are obtained with a Schmidt-Cassegrain telescope of focal ratio f/10 and diameter $D = 40.64$ cm and installed on an equatorial mount, manufactured by Meade. The optics consists of two achromatic lenses of 50 mm focal-length. With this optical arrangement, the virtual analysis plane is located 1.94 km below the pupil. The diameter of the pupil image on the detector is $D' = 24.5$ mm. The scintillation images are captured by an EMCCD camera (Andor iXon) with 512×512 square pixels of 16 μm. The frames are binned 2×2, and the active zone is limited to an array of 256×80 binned pixels. The exposure time of each frame ranges from 3 to 10 ms, depending on the wind conditions. The typical number of images to obtain one autocovariance is set to 30000.

The EMCCD camera is mounted on a base that is attached to the rear of the telescope (see Fig. 2). The same equipment, but with different optics, is used to form the SLODAR instrument. To switch between each instrument with the required positioning accuracy, a manual exchange mechanism was installed in front of the camera.

3.2. *Second generation*

As seen in Fig. 3, LOLAS-2 uses a Ritchey-Chrétien open telescope of focal ratio f/9 and diameter $D = 40.64$ cm, manufactured by RC Optical Systems, a German equatorial mount (1200GTO) manufactured by Astro-Physics, an EMCCD camera (Andor iXon) to acquire scintillation images and a Sbig St-402ME camera for the finder telescope.

One advantage of using a Ritchey-Chrétien telescope is that when the position of the focal plane

is changed, the effective focal length of the telescope remains unchanged. Our RC Optical Systems telescope is equipped with a system that maintains the focus by monitoring the secondary mirror position in closed loop at a frequency of 6 kHz, reaching an accuracy in the secondary mirror and the focus positions of 0.6 and 25.4 μm, respectively. This control system is part of the telescope. In addition, the fact that the telescope is open prevents air at different temperatures to get trapped inside the tube in a turbulent convective flow, which would add an instrumental bias to the C_{N}^2 measurements at ground level. This was the case with the prototype LOLAS. Removal of the spurious turbulence from the measurements was performed in a post-processing procedure using the method described by Avila et al. (2001), as reported by Chun et al. (2009). In LOLAS-2, this post-processing step is avoided, making the data reduction faster and simpler.

Concerning the mount, LOLAS-2 incorporates a German-type mount that reduces considerably the lever arm between the equatorial and declination axis. Moreover, the Astro-Physics mount has a higher stiffness and the worm gear accuracy is significantly better, compared to those of the Meade mount.

The prototype version uses the optics of the telescope and achromatic doublets to define the spatial sampling and conjugation distance h_{gs} below the pupil. The second generation instrument was developed so as to dispense the use of the achromatic doublets and the exchange mechanism. It only uses the telescope optics, making it a simpler and more robust instrument. The beam is no longer collimated, like in the prototype version. The EMCDD is placed directly a distance L before the telescope focal plane. Distance L is chosen such that the detector plane is made the conjugate of the a virtual plane located a distance h_{gs} below the telescope pupil (see Fig. 4*a*) and the spatial sampling on this plane is well-suited to sample the scintillation speckles (see Fig. 4*b*). Using the thin

lens equation, it can easily be shown that $h_{\rm gs}$ is related to L by the following expression:

$$h_{\rm gs} = -\frac{{F_{\rm tel}}^2 - F_{\rm tel}L}{L}, \tag{1}$$

where $F_{\rm tel}$ is the focal length of the telescope. For the spatial sampling, Fig. 4*b* illustrates the demagnification relation:

$$\frac{\mathcal{L}_D}{L} = \frac{\mathcal{L}_{\rm min}}{F_{\rm tel}} \tag{2}$$

where $\mathcal{L}_{\rm min}$ represents the typical size of the smallest scintillation speckles on the pupil and $\mathcal{L}_D$ is its corresponding size on the detector plane. Prieur et al. (2001) showed that the full width at half maximum of the autocovariance of the scintillation produced at altitude h is given by

$$\mathcal{L}(h) = 0.78\sqrt{\lambda|h - h_{\rm gs}|}). \tag{3}$$

This is, the typical size of the smallest speckle is $\mathcal{L}_{\rm min} \equiv \mathcal{L}(0) = 0.78\sqrt{\lambda|h_{\rm gs}|}$. Solving Eq. 2 for $\mathcal{L}_D$ and replacing the above expression for $\mathcal{L}_{\rm min}$ gives:

$$\mathcal{L}_D = L\frac{0.78\sqrt{\lambda|h_{\rm gs}|}}{F_{\rm tel}}. \tag{4}$$

For ground-level turbulence to be detectable, $h_{\rm gs}$ must be smaller than -1000 m. A good spatial sampling of the scintillation speckles is obtained when $\mathcal{L}_D \simeq 2p$, where p is the size of the elementary sampling element. We chose to acquire images with the camera pixels binned 2×2. In that case, $p = 2d_{\rm pix}$. The camera pixel size is $d_{\rm pix} = 16$ μm. Table 1 gives values of different parameters of interest for different values of L. It can be seen that a good compromise is obtained when the detector is located a distance $L = 11$ mm before the telescope focal plane, as the conjugation distance is large enough ($h_{\rm gs} = -1212$ m) and the number of spatial samples per smallest speckle width is 1.8, which is very close to 2, the Nyquist criterion. Even though the undersampling is small, it is taken into account in the kernel of the inversion process that calculates $C_{\rm N}^2$ profiles from the measured autocovariances.

As a consequence of this analysis, the value for L is set to 11 mm in LOLAS-2. For this value of L, the distance separating two contiguous binned pixels corresponds to an angular separation of $1.8''$.

4. INSTRUMENT PERFORMANCE

In this section we present results concerning the focus stability and guiding performance obtained the Observatorio Astronómico Nacional at San Pedro Mártir (OAN-SPM), Baja California, Mexico. The data was obtained on the nights of 2013 June 15, 16 and 17. Table 2 summarises the pertinent characteristics of the double-star targets used.

4.1. *Focus stability*

Focus stability is extremely important to maintain the spatial sampling and conjugation altitude along data acquisition. A variation of the telescope focus position translates into a variation of the pupil image diameter d on the detector. This diameter is continuously monitored during the standard data acquisition of the instrument. Images are sent by the EMCCD to the computer in packets of 200 consecutive 256x80 pixels frames. In each frame, the image is centred (as explained in §4.2) and then co-added to form a mean image made of 200 frames. The pupil diameters are calculated from this mean image as follows (see Fig. 5): the mean image is integrated along columns to form a row of the accumulated values. The width at half maximum of the left and right pupils on the accumulated-values row determines their diameter in number of pixels $N_{d,l}$ and $N_{d,r}$, respectively.

To estimate the focus stability, the diameter of each pupil was monitored during several hours on three nights, using the same double star as source. The total number of pupil size measurements was 4566. The mean and standard deviation of the measured diameters are $\langle N_d \rangle = 38.13$ and $\sigma_{N_d} = 0.40$ pixels. The average of the temperature and its variation for each night was 13.5 ± 0.22, 14.6 ± 0.23 and 14.1 ± 0.07 Celcius degrees, according to the weather station at SPM. The obtained standard deviations can be due to uncertainties in the estimation procedure and/or to actual physical variation

in the focus or camera positions. If we consider the latter to be the cause of the measured diameter fluctuations, the consequence of the deviation of 0.40 pixels in pupil diameter implies a variation of 13 m in altitude conjugation and 0.32 μm in the sampling element size on the detector, approximately, which are tolerable values. This result suggests that the use of an auto-focus algorithm, which was developed for the prototype LOLAS, could be avoided in the second generation instrument, although more tests under varying temperature conditions should be performed.

4.2. *Guiding test*

Maintaining a constant position of the pupil images on the EMCCD is important to correctly compute the mean image, the autocorrelation of which is used to normalize the mean autocorrelation of scintillation images, so obtaining the scintillation autocovariance. On wind conditions commonly encountered in astronomical observatories, telescope shake may cause pupil images to move on the detector. This eventual image wander is corrected for by centering the image in every single frame captured by the detector. The guiding performance of the telescope mount is important to keep pupil images within the useful window of the EMCCD during data acquisition that may last hours.

The image position on the active area of the EMCCD is determined as follows: we construct an artificial reference image $I_{\rm r}(\mathbf{r})$ formed by two disks of 38 pixels in diameter each and separated from each other by the same distance as the observed double star. We compute the cross-correlation $C_{\rm c}(\mathbf{r})$ of the current image $I_i(\mathbf{r})$ with $I_{\rm r}(\mathbf{r})$. The position of the pupil images (X, Y) in $I_i(\mathbf{r})$ is set as the position of the maximum value of $C_{\rm c}(\mathbf{r})$ with respect the frame centre.

In standard operation of LOLAS-2, image positions are not saved on disk. To test the guiding performance and image stability we recorded image positions (X, Y) during several observations. The (X, Y) coordinates on the EMCCD were rotated according to the double-star position angle to obtain image positions in right ascension (α) and declination (δ) coordinates system. This allows us

to investigate separately the guiding and stability behaviour on the two rotation axis of the mount. Figures 6 and 7 show two examples. For the results obtained on 2013 June 17 UT (Fig. 6) wind was blowing from the South-West with mean speed of 15.5 km h^{-1} and a maximum value of 18.0 km h^{-1}. The image positions remained very stable apart from a slow continuous drift on δ and a slow oscillation in α, presumably due to an inexact alignment of the mount and a periodic error on the right-ascension gear-mechanism, respectively. On 2013 June 15 UT wind was less benevolent, blowing from the West at a mean speed of 26.6 km h^{-1} with gusts reaching 40 km h^{-1}. Figure 7 shows an example of that night. Even though images were moving significantly, the mean position remained constant and pupil images remained within the EMCCD working window, which enabled turbulence profiles to be measured in these conditions.

To investigate further the dependence of image jitter on prevailing wind speed, in Fig. 8 it is shown a plot of the standard deviation of image position as a function of wind speed. For each of the available 4566 frame-packets, the standard deviation σ_η of the image position was calculated. The frame rate within each packet is 13-ms per frame. The wind conditions that prevailed at the time of each measurement were obtained from the database of the OAN-SPM weather station[1]. Bar extremities on Fig. 8 indicate the 25 and 75 percentiles of the σ_η values for a given wind speed. As expected, strong winds produce large image jitter, but surprisingly, σ_η values remain lower than $5''$ for wind speeds lower than 30 ms^{-1}. Even though the force exerted by the wind on the telescope is proportional to the wind speed, the mount and telescope structures move significantly only if the wind speed exceeds a certain value that seems to lie between 30 and 35 ms^{-1}.

The telescope and mount stiffness, together with the guiding performance have proven to suffice for conducting observations in moderate to strong wind conditions, without the need of an auto guiding

[1] www.astrossp.unam.mx/weather15/

procedure like in the prototype LOLAS.

5. C_N^2 MEASUREMENT EXAMPLES

In this section we present a few examples of measured scintillation autocorrelations and corresponding turbulence profiles. The first results of LOLAS-2 were obtained in 2013 November at the OAN-SPM. The instrument was installed on a concrete pillar (see Fig. 3) to reduce vibrations.

Figure 9 shows examples of autocovariance maps obtained from 30 000 scintillation images, during the nights 2013 November 16 and 17. In the central peaks of Figs. 9*a* and 9*c* , the contribution of all turbulent layers in the atmosphere are added up. The correlated speckles produced by turbulent layers above h_{max} are separated by a distance longer than the pupil diameter, thereby not giving rise to lateral peaks inside the autocovariance-map boundaries and avoiding the corresponding C_N^2 estimate. Only the layers below h_{max} form visible lateral peaks from which C_N^2 values are retrieved. A white rectangle frames the right-hand side lateral peaks in Figs. 9*a* and 9*c*. Enlarged views are shown in Fig. 9*b* and 9*d*. The most intense central peak inside each of those frames corresponds to the turbulence at ground level. Weaker peaks can clearly be seen in Fig. 9*a*, which correspond to turbulence above the ground. Fig. 9*d* only exhibits ground-level turbulence.

The $C_N^2(h)$ profiles are obtained using a modified CLEAN algorithm (Avila et al. 2008) based on the one presented by Prieur et al. (2001). In Fig. 10 we present a few profiles obtained on 2013 November 16 and 17 using autocovariance maps whose examples are shown in Fig 9. The purpose of Fig. 10 is only to display the ability of the instrument in measuring C_N^2 profiles and their characteristics. It is not intended for studying the optical turbulence at the site. Altitude resolution, maximum sensed altitude and noise level values are summarised in Table 3. Note that the altitude resolution obtained when using 12 Cam as a target is the best ever achieved with Scidar-like techniques. The noise levels indicated in Table 3 are the C_N^2 values that correspond to the 3σ, i.e. three times the standard

deviation on the autocovariance-map background (Avila et al. 2008). The profiles corresponding to November 16 show three turbulent layers: one at ground level, the second at 81 m and the weakest at 390 m. On November 17, almost all turbulence below 400 m was concentrated at ground level. Only a weak turbulent layer is detected at 170 m above the ground at 11:27 UT that night. It is worth recalling that C_N^2 values obtained with Scidar techniques in which the pupil images are not superimposed on the detector, like LOLAS, do not need to be corrected for the normalization error pointed out by Avila & Cuevas (2009).

6. CONCLUSIONS

The second generation of the Low Layer Scidar incorporates a simplified optical layout, a stiff and precise telescope mount and an open Ritchey-Chrétien telescope with excellent focus stability. The analysis of the image positions showed that the guiding quality of the mount permits to avoid the autoguiding algorithm that was used in the prototype LOLAS. Similarly, the excellent focus stability of the telescope allows for observations without the autofocus algorithm employed in the former version of the instrument. Examples of measurements obtained with LOLAS-2 illustrate the capability of the instrument for very high altitude-resolution profiling of the optical turbulence. A statistical analysis of $C_N^2(h)$ profiles obtained so far at the OAN-SPM will be presented in a forthcoming paper.

We are deeply grateful to the staff of the Observatorio Astronómico Nacional at San Pedro Mártir (OAN-SPM) for their kind help in all the logistics for the observations. Wind data used in the work was provided by the OAN-SPM wheather station (http://tango.astrosen.unam.mx). Financial support was provided by DGAPA–UNAM through grants IN103913 and IN115013.

REFERENCES

Avila, R., Avilés, J. L., Wilson, R. W., Chun, M., Butterley, T., & Carrasco, E. 2008, MNRAS, 387, 1511

Avila, R. & Cuevas, S. 2009, Optics Express, 17, 10926

Avila, R., Masciadri, E., Vernin, J., & Sánchez, L. 2004, PASP, 116, 682

Avila, R., Vernin, J., & Masciadri, E. 1997, ApOpt, 36, 7898

Avila, R., Vernin, J., & Sánchez, L. J. 2001, A&A, 369, 364

Avilés, J. L., Avila, R., Butterley, T., Wilson, R., Chun, M., Carrasco, E., Farah, A., & Cuevas, S. 2012, MNRAS, 423, 900

Chun, M. 1998, PASP, 110, 317

Chun, M., Wilson, R., Avila, R., Butterley, T., Aviles, J.-L., Wier, D., & Benigni, S. 2009, MNRAS, 394, 1121

Egner, S. E. & Masciadri, E. 2007, PASP, 119, 1441

Fuchs, A., Tallon, M., & Vernin, J. 1998, PASP, 110, 86

Le Louarn, M. & Hubin, N. 2006, MNRAS, 365, 1324

Osborn, J., Wilson, R., Butterley, T., Shepherd, H., & Sarazin, M. 2010, MNRAS, 406, 1405

Prieur, J.-L., Daigne, G., & Avila, R. 2001, A&A, 371, 366

Rigaut, F. 2002, in Beyond conventional adaptive optics, ed. E. Vernet, R. Ragazzoni, S. Esposito, & N. Hubin, Vol. 58 (ESO Conference and Workshop Proceedings), 11–16

Rocca, A., Roddier, F., & Vernin, J. 1974, Journal of the Optical Society of America (1917-1983), 64, 1000

Schöck, M., Els, S., Riddle, R., Skidmore, W., Travouillon, T., Blum, R., Bustos, E., Chanan, G., Djorgovski, S. G., Gillett, P., Gregory, B., Nelson, J., Otárola, A., Seguel, J., Vasquez, J., Walker, A., Walker, D., & Wang, L. 2009, PASP, 121, 384

Shepherd, H. W., Osborn, J., Wilson, R. W., Butterley, T., Avila, R., Dhillon, V. S., & Morris, T. J. 2014, MNRAS, 437, 3568

Tokovinin, A. 2004, PASP, 116, 941

Tokovinin, A., Bustos, E., & Berdja, A. 2010, MNRAS, 404, 1186

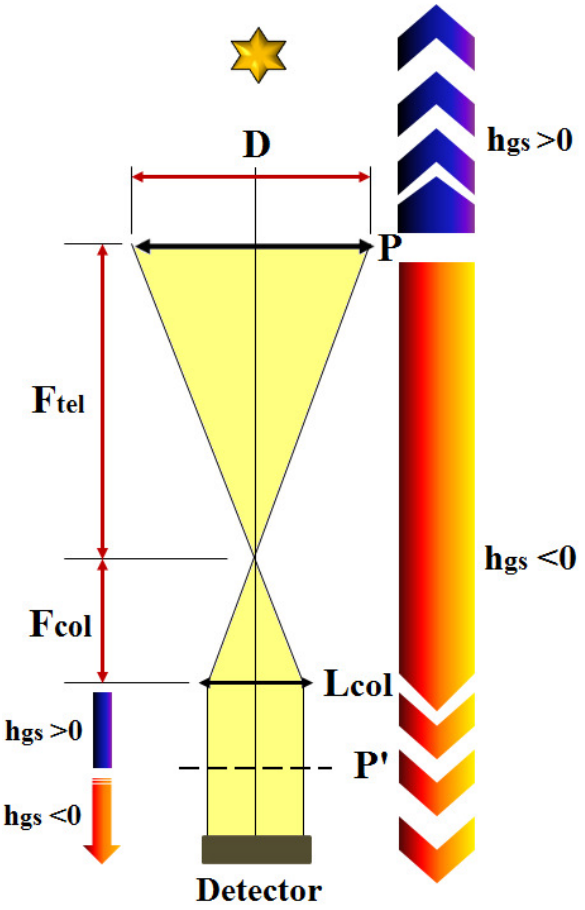

Figure 1. Optical layout of the G-SCIDAR.

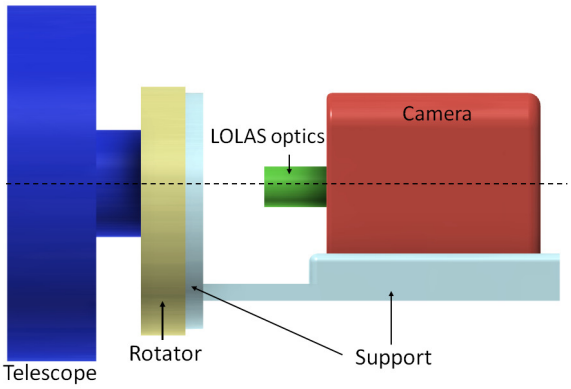

Figure 2. Schematic view of the prototype LOLAS instrument.

Figure 3. LOLAS-2 at the Observatorio Astronómico Nacional de San Pedro Mártir (OAN-SPM).

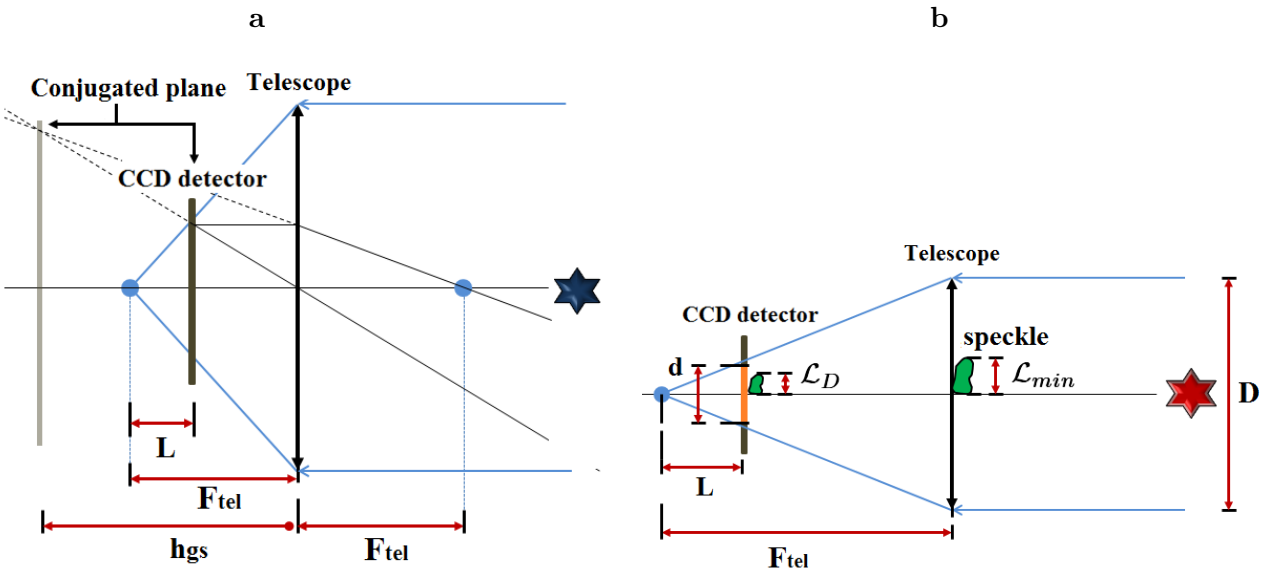

Figure 4. (a) Optical scheme of LOLAS-2. When the CCD is placed before the focal point of the telescope, its conjugate plane is located a distance $h_{\rm gs}$ underneath the pupil ($h_{\rm gs} < 0$), (b) Scheme showing the geometrical relations that lead to Eq. 2.

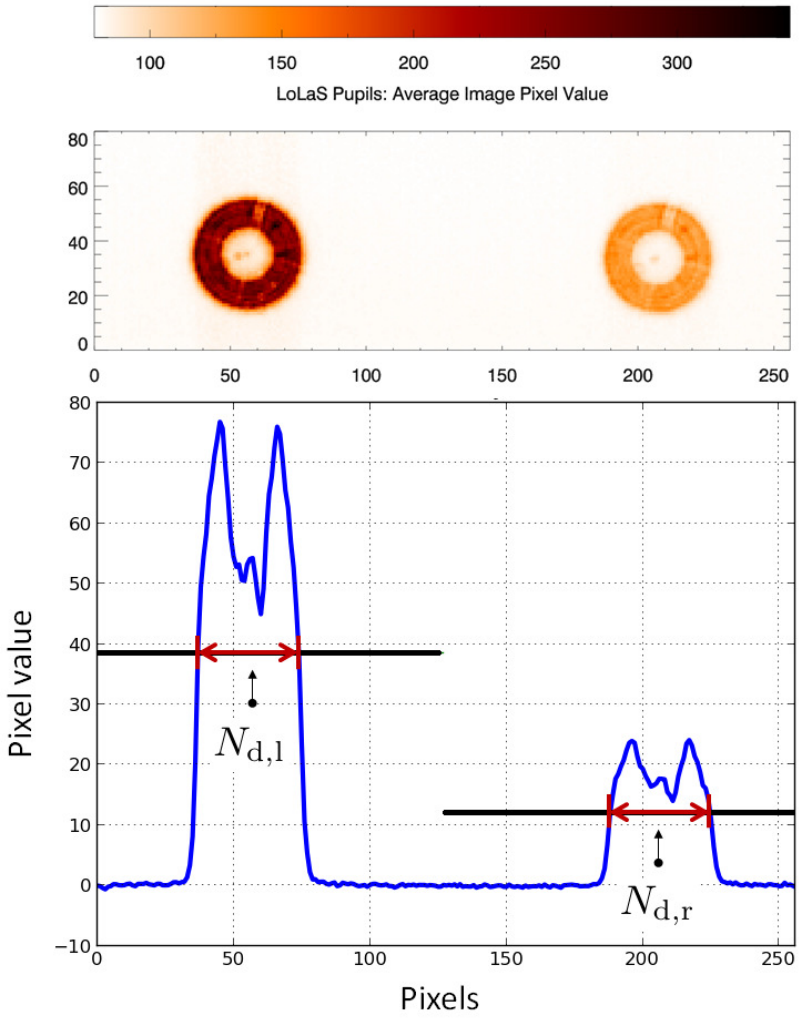

Figure 5. Average image for the calculation of pupil diameters $N_{d,l}$ and $N_{d,r}$ in pixels.

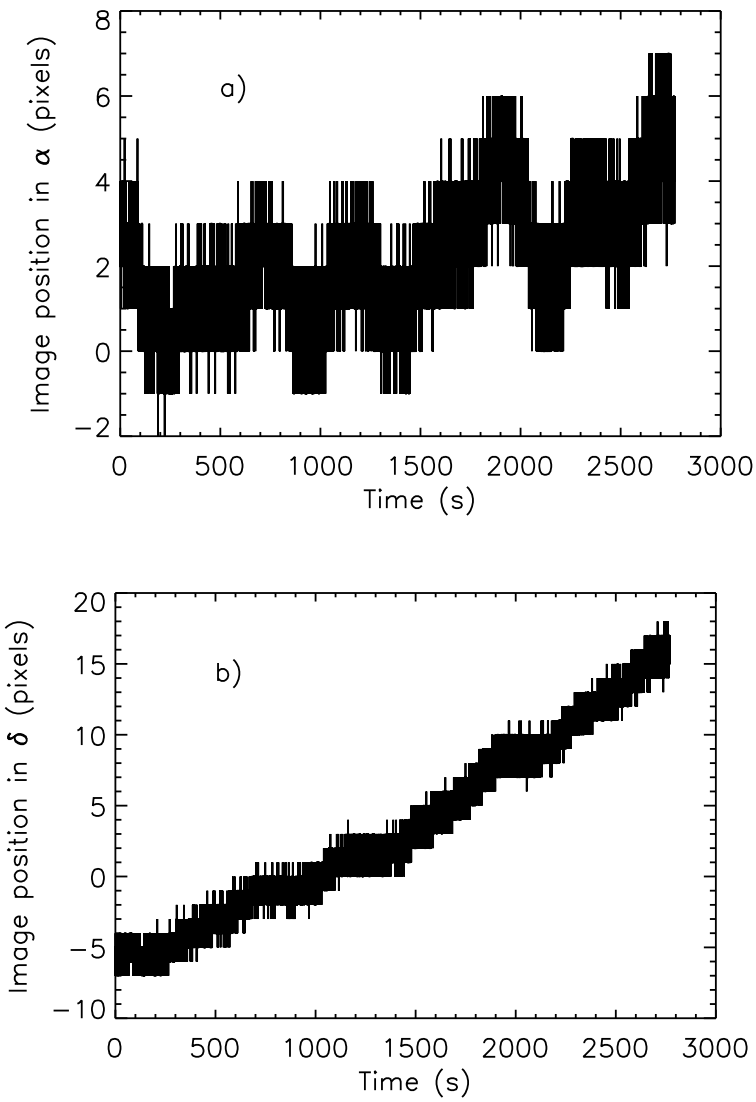

Figure 6. Example of recorded image positions in pixels with respect to the EMCCD centre as a function of time, along right ascension (a) and declination (b) directions, respectively. Data were obtained on 2014 June 15.

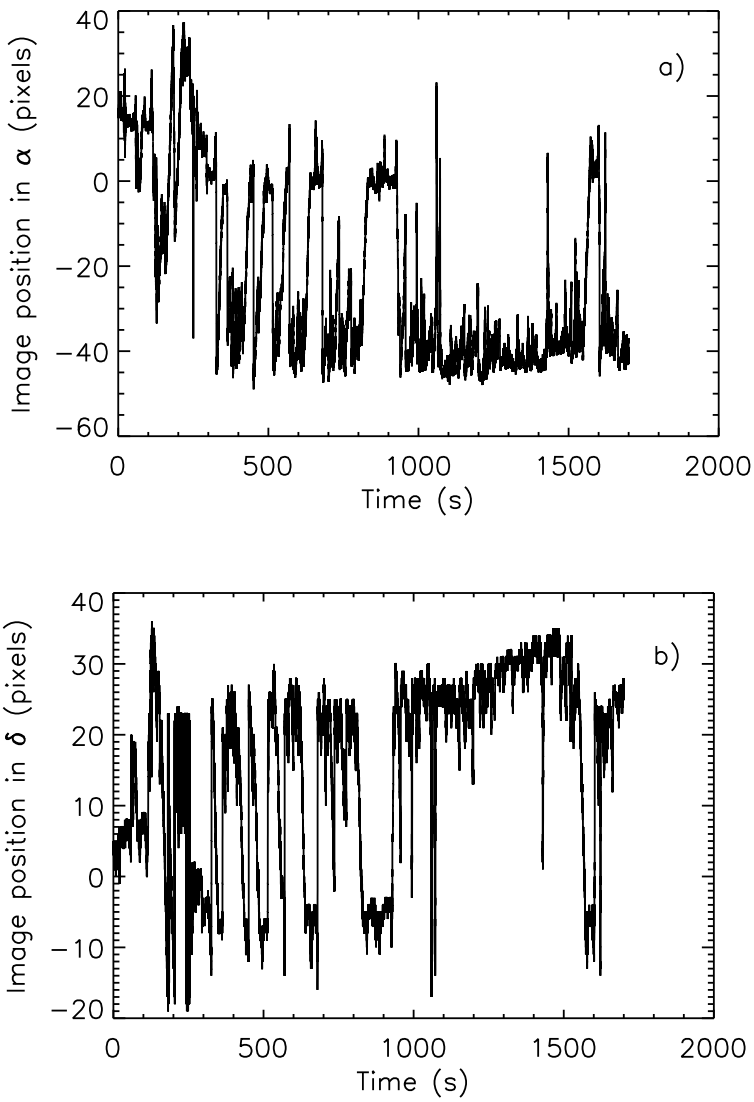

Figure 7. Similar to Fig. 6 for data obtained on 2014 June 17.

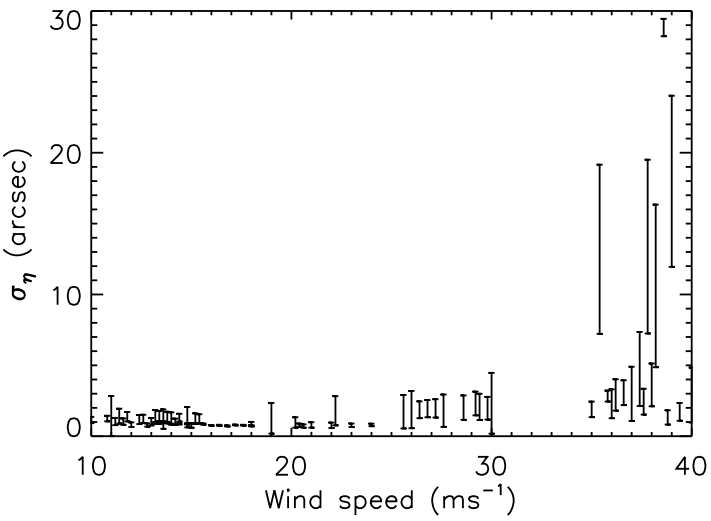

Figure 8. Image jitter as a function of wind speed. Bars indicate the 25 and 75 percentiles of the image jitter (standard deviation of image position) values measured under a given value of wind speed.

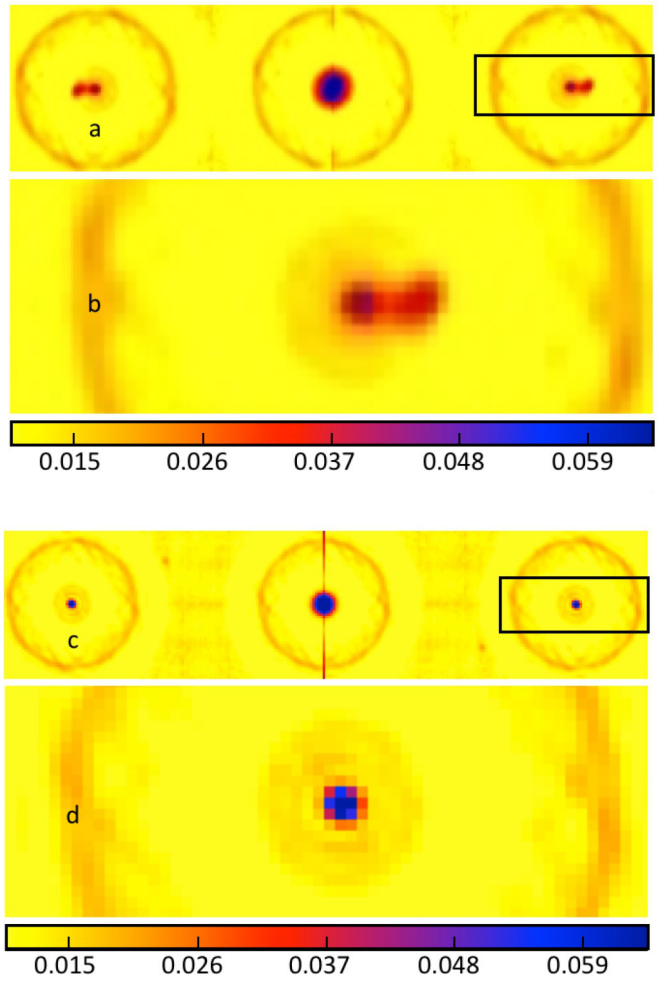

Figure 9. Examples of measured autocovariance maps. Data were obtained at the OAN-SPM on 2013 November 16 at 5:43 UT with the double star 15 Tri (*a* and *b*) and on 2013 November 17 at 9:36 UT using target 12 Cam (*c* and *d*). Frames *b* and *d* show enlarged views of the rectangles that appear in frames *a* and *c*.

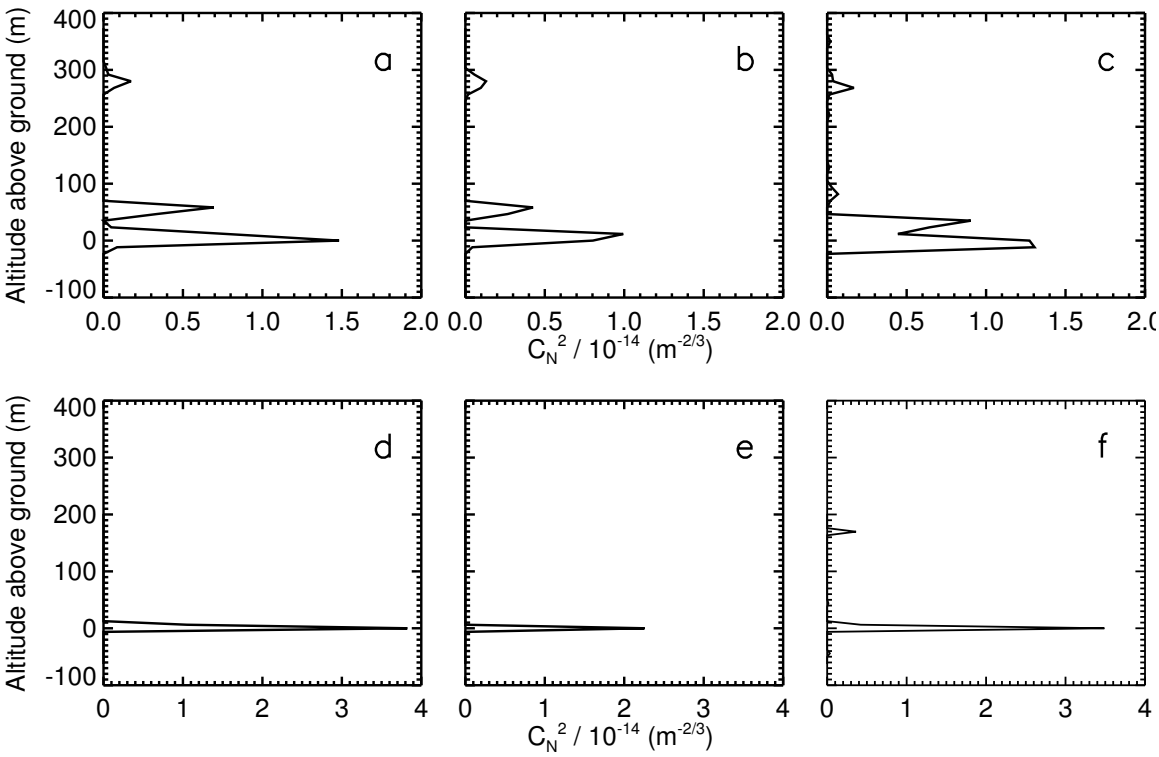

Figure 10. Examples of C_N^2 profiles obtained at the OAN-SPM on 2013 November 16 at 5:43 *a* , 5:47 (*b*) and 10:10 (*c*) and on 2013 November 17 at 9:36 (*d*) , 10:27 (*e*) and 11:27 (*f*) . Dates and times are in UT.

Table 1. Instrumental parameters for different values of L

Parameter	L_1=15 mm	$\boldsymbol{L_2}$ **=11 mm**	L_3=7.5 mm	L_4=5 mm
$h_{\rm gs}$[m]	-886	**-1212**	-1777	-2668
d [mm][a]	1.66	**1.22**	0.83	0.55
N_d [pixels][b]	52	**38**	26	17
$\mathcal{L}_D/p$[c]	2.58	**1.80**	1.29	0.86

[a] Diameter of the pupil image on the detector plane.

[b] Number of binned pixels along a pupil image diameter (Fig. 5).

[c] Number of binned pixels along a speckle (for $h = 0$).

Table 2. Targets

Name	α_{2000}[a]	δ_{2000}[a]	m_1[b]	m_2[b]	ρ[c] [$''$]
15 Tri	2^h:35	34°:41	5.5	6.7	138.9
12 Cam	5^h:06	58°:58	5.2	6.2	181.3

[a] Right ascension (α_{2000}) and Declination (δ_{2000}).

[b] Visible magnitude of each star.

[c] Angular separation.

Table 3. Observational parameters

Date	Target	Δh[a]	$h_{\max}$[b]	τ[c]	N. L.[d]
2013/11/16	15 Tri	11.7	603	3	9.5×10^{-16}
2013/11/17	12 Cam	6.3	462	2	1.3×10^{-15}

[a] Altitude resolution [m].

[b] Maximum altitude [m].

[c] Exposure time [ms].

[d] Noise level [$m^{-2/3}$].